Higher order correlation detection in nonlinear aerodynamic systems using wavelet transforms

K. Gurley
Department of Civil and Coastal Engineering, University of Florida, USA

T. Kijewski & A. Kareem
Department of Civil Engineering and Geological Sciences, University of Notre Dame, USA

Keywords: coherence, bicoherence, wavelet transform, correlation detection, scalogram

ABSTRACT: The wavelet transform technique is used to detect intermittent linear and higher order correlation between pairs of correlated random signals. The statistical relevance of the resulting time dependent coherence and bicoherence are analyzed in light of the inherent noise in estimates. The presence of intermittent correlation is delineated from uncorrelated regions through the use of reference maps of likely statistical noise between uncorrelated simulated signals.

1 INTRODUCTION

The increasing use of wavelet transform-based methods in signal analysis results from their ability to display time and frequency information independently, usually in the form of a variance map with respect to time and scale (e.g. Kareem et al. 1993). Wavelets are now being used in a wide array of applications in engineering disciplines where transients shape the signature characteristics (e.g. Farge 1992, Dunyak 1997, Gurley & Kareem 1999).

This study uses wavelet transforms to identify the first and higher-order intermittent correlation between measured records. The wavelet transform is used in place of the Fourier transform to estimate the coherence and bicoherence. This allows a display of coherence and bicoherence in terms of time and frequency, revealing linear and second-order intermittent relationships. The influence of noise in the estimation of coherence and bicoherence over a localized time frame is significant, making a distinction between the true correlation and noise a major issue that needs to be addressed. A method for establishing a threshold for statistically meaningful coherence and bicoherence through reference distributions is developed. Independent realizations of time histories that match the power spectrum and probability contents of the signals being analyzed are simulated to establish a statistical measure of the expected noise in the estimated coherence and bicoherence. By comparing these reference distributions with those of the measured data, meaningful linear and higher-order coherence can be identified. A quantitative measure of the statistical significance is established through non-Gaussian probability models.

2 WAVELET COHERENCE MAP

2.1 *Wavelet background – scalogram and coscalogram*

Wavelet analysis decomposes a signal into a set of finite basis functions. Consequently, wavelet analysis can uncover transient characteristics obscured by the infinite sinusoidal basis functions used in Fourier analysis. Wavelet coefficients $W_x(a,t)$ are produced through the convolution of a parent wavelet function $y(t)$ with the analyzed signal $x(t)$

$$W_x(a,t) = \frac{1}{\sqrt{|a|}} \int x(t) y\left(\frac{t-t}{a}\right) dt \quad . \tag{1}$$

The parent wavelet used in this study is the Morlet wavelet, defined along with its scale/frequency relationship as (Misiti et al. 1996)

$$y(t) = \exp\left(\frac{-t^2}{2}\right)\cos(5t), \qquad \text{where} \quad f \cong \frac{5}{2pa} \tag{2 a,b}$$

a and t denote the scale and local time center of the analyzing wavelet. This well-defined relationship between scale and frequency makes the Morlet wavelet an attractive choice for this study. Excellent resources are available for a rigorous mathematical presentation of the wavelet transform (e.g. Daubechies 1988, Strang & Nguyen 1996).

The localized wavelet coefficients are well suited for analyzing non-stationary events such as transient and evolutionary phenomena. When the squared coefficients are plotted on a time-scale grid, the transfer of energy from one band to the next may be observed along the time scale. This is called the scalogram or mean square map. Some recent studies have used a variation of the scalogram to identify correlation between signals (e.g. Gurley et al. 1997). The squared coefficient value is replaced with the product of the wavelet coefficients of two different processes. This coscalogram produces a view of the coincident events between the processes, revealing time varying pockets of correlation over frequency.

Pressure measured on the rooftop of a full-scale building and wind velocity fluctuations measured upstream of the building are utilized to demonstrate the coscalogram. The scalogram of wind velocity and simultaneously measured pressure are presented along with their coscalogram in the three plots in the left column of Figure 1. Dark patches in the coscalogram identify areas of correlation. The right column of Figure 1 presents the same information for two uncorrelated records. The resulting coscalogram of these two unrelated processes in the bottom right corner shows no distinct correlation. This concept has been used to qualitatively identify first-order wind velocity and pressure relationships (Gurley & Kareem 1999). The cospectrum contains wavelet coefficients determined from segments of the signal isolated by the sliding window specified by the mother wavelet. As a result, a given segment will have significant overlap with previous and subsequent analysis segments. At each time step, the wavelet coefficients comprise a single raw spectrum across the range of scales, equivalent to a spectrum obtained from a single time history in the traditional FFT analysis. These raw spectra that comprise the cospectrum lack the ensemble averaging necessary in traditional Fourier methods. This produces noisy displays where correlated events are difficult to differentiate from random coincident coefficients.

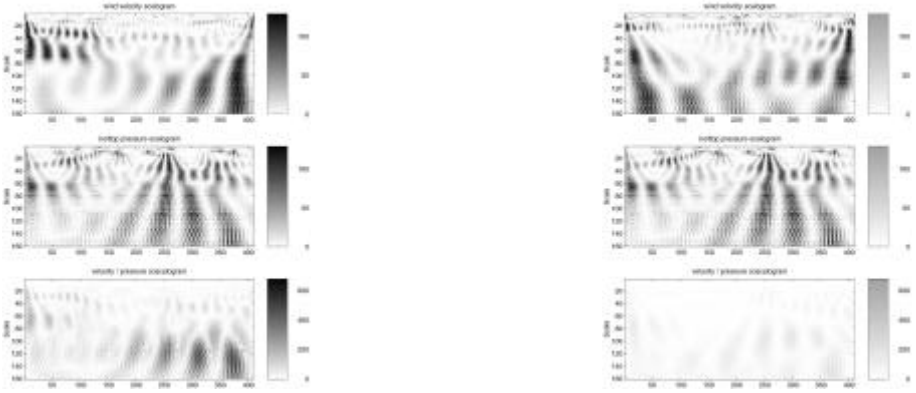

Figure 1. Left: top to bottom - scalogram of upstream wind velocity and correlated rooftop pressure, and coscalogram of these two processes. Right: top to bottom - scalogram of uncorrelated wind velocity and pressure records, and the coscalogram of these two records.

Other studies have applied higher-order spectral analysis to quantify the nonlinear relationship between wind velocity and pressure (Gurley et al. 1997). These Fourier transform-based higher-order spectral methods are not capable of capturing the transient intermittent relationship being sought here. A more accurate and reliable approach to quantitatively identify intermittent first and higher-order correlation is the thrust of this study.

2.2 *Coherence map derivation*

The time-frequency wavelet-based coherence map follows the form of the Fourier-based coherence function: the ratio of the cross spectrum to the product of the auto-spectra of the two signals $x(t)$ and $y(t)$. The wavelet coherence is

$$\left(c^W(a,t)\right)^2 = \frac{\left|S_{xy}^W(a,t)\right|^2}{S_{xx}^W(a,t)S_{yy}^W(a,t)}, \tag{3}$$

where the localized power spectra above are

$$S_{ij}^W(a,t) = \int_T W_i^*(a,t)W_j(a,t)dt \ . \tag{4}$$

The localized time integration window in Equation 4, $T = [t-\Delta t, t+\Delta t]$, is selected based on the time resolution desired in the resulting coherence map. The integration effectively provides an ensemble averaging localized in time. The map is bounded between 0 and 1, and provides a view of the localized correlation with respect to both time and frequency.

2.3 *Comparison of wavelet-and Fourier-based coherence estimates*

The validity of the coherence map in Equations 3-4 is demonstrated by first applying the wavelet based coherence to stationary signals. The standard Fourier-based coherence estimate is directly compared with the wavelet-based coherence by averaging out the time information in the wavelet coherence map

$$\left(c^W(a)\right)^2 = \frac{1}{nt}\sum_{i=1}^{nt}\left(c(a,t_i)\right)^2 \tag{5}$$

where nt is the number of discrete time steps resulting from the localized time window.

The signals being analyzed are upstream wave elevation and the resulting surge response of a 1:200 scale model of a tension leg offshore platform (TLP) (Fig. 2). 4096 seconds of data are used in this analysis, sampled at 1 Hertz. The measurements were taken in a controlled laboratory environment as part of another study (Vickery 1988). Equations 1-4 are applied to these signals with the results shown in Figure 2 (right, top). The coherence is well represented by both estimates, demonstrating the accuracy of the wavelet-based coherence estimate with respect to both magnitude and frequency. A second example demonstrates that wavelet-based coherence can accurately estimate smaller levels of linear correlation. Independent white noise vectors are added to the wave and TLP response time histories to reduce the level of correlation, and coherence estimates are again produced. Figure 2 (right bottom) shows the wavelet coherence representing correlation accurately.

2.4 *Filtered wavelet coherence map*

The coherence map in Equations 3-4 produces a display with considerable noise, making statistically significant correlation difficult to interpret. Ridge extraction techniques have been effectively used for detection of a limited class of signals in noise (e.g. Carmona et al. 1998). In this study we present a more brute force approach appropriate for a wide class of signals with

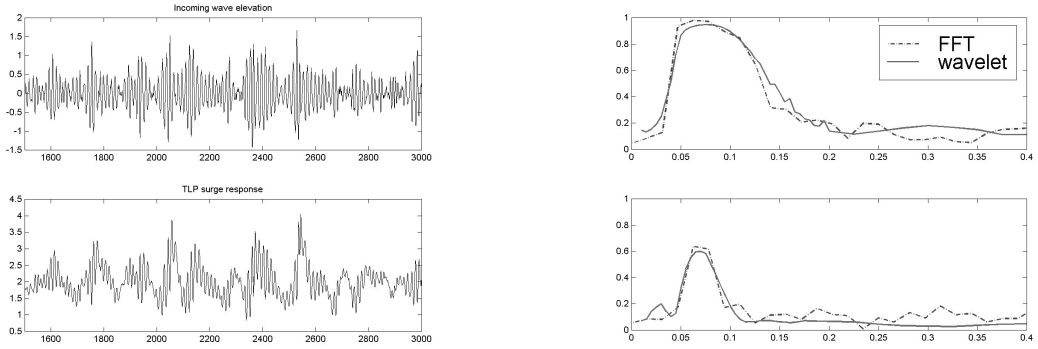

Figure 2. Left: Wave elevation (top), TLP response (bottom). Right: Wavelet and FFT coherence estimates between original signals (top), Wavelet and FFT coherence estimates between signals with incoherent noise added to each (bottom).

transient behavior. In order to separate statistically relevant correlations from spurious peaks, a reference map describing the expected noise threshold in the correlation display is generated.

Coherence maps are created between the first signal $x(t)$ and multiple simulations of the second signal, denoted $y_s(t)$. These simulated signals are independent of each other and $x(t)$ and are statistically identical to the original signal $y(t)$ in both the power spectral density (PSD) and probability density function (PDF) through the use of a recently developed non-Gaussian simulation algorithm (Gurley & Kareem 1997a).

A wavelet noise coherence map between $x(t)$ and $y_s(t)$ is produced for each of the N independent simulations, delineated $\left(c_{mn}(a,t)\right)^2$. These maps are then averaged to produce a mean noise reference map

$$\left(c_{mn}(a,t)\right)^2 = \frac{1}{N}\sum_{i=1}^{N}\left(c_i^{nc}\ (a,t)\right)^2 \tag{6}$$

where N is the number of simulated uncorrelated pressure records. The standard deviation of the reference maps is also calculated, $c_{st}(a,t)$. The threshold value of a statistically meaningful correlation is then the sum of this mean and the standard deviation weighted by a factor *g*

$$c_{th}(a,t) = c_{mn}(a,t) + g\left(c_{st}(a,t)\right). \tag{7}$$

The factor g is selected based on the desired probability of exceeding the noise threshold. A quantitative approach is discussed after an example application of the noise threshold. The results of equation 3 are subjected to the threshold determined by equation 7 and a filtered coherence map is generated according to

$$c_F^W(a,t) = \begin{Bmatrix} 0 & if \quad c^W(a,t) < c_{th}(a,t) \\ c^W(a,t) & if \quad c^W(a,t) > c_{th}(a,t) \end{Bmatrix}. \tag{8}$$

To demonstrate the methodology, velocity and pressure signals with known pockets of short duration correlation over selected frequency ranges are created. Two independent Gaussian wind velocity signals $(u_1(t), u_2(t))$ are simulated based on a target wind spectrum. Each velocity record is 2048 seconds long, sampled at one Hertz. The pressure record is created by combining white noise $(e(t))$ with the two wind records. Band pass filtering is used to correlate velocity to pressure only over selected frequency ranges. The pressure record is related to the second wind record and the noise by

$$pr(t) = e(t) + u_2(t) + G(e(t)^2 + u_2(t)^2) \tag{9}$$

For this example $G = 0.05$. Two small segments of the pressure are then replaced with signals generated by the same equation, except with the first wind record replacing n_2

$$pr(t) = e(t) + u_{1f}(t) + G(e(t)^2 + u_{1f2}(t)^2), \tag{10}$$

where $n_{1_f}(t)$ indicates $n_1(t)$ after band pass filtering is applied. t represents time segments from 512 to 768 seconds and from 1536 to 1792 seconds. Using the filtered wind velocity record in Equation 10 produces a pair of signals, $pr(t)$ and $n_1(t)$, correlated from 512 to 768 seconds between 0.0625 and 0.25 hertz, from 1536 to 1792 seconds between 0.19 and 0.37 hertz, and uncorrelated everywhere else.

The wavelet-coherence map in Equation 3 is applied to determine the coherence between $n_1(t)$ and $pr(t)$ in Figure 3 (left). A time integration window of 64 seconds was applied. Pockets of higher correlation can be identified in these displays, including the time and frequency regions of known correlation discussed after Equation 10. However, the raw coherence map estimate displays spurious correlation. Figure 3 (right) shows the filtered coherence map after application of Equation 8 filters out noise with 100 simulations. The correlated features are clearly seen in the two views of the filtered coherence map, while most extraneous noise is eliminated.

The noise factor g in Equation 7 is selected based on the probability distribution of the noise coherence maps. Higher-order statistics are collected from the multiple noise maps in addition to their mean and standard deviation. The first four moments are used to fit a non-Gaussian probability distribution to the random noise map (Gurley & Kareem 1997b). The tail region of the resulting PDF model of the noise map then represents the probability of noise exceeding the selected threshold that demarcates correlation in the wavelet coherence map. The noise factor g, in Equation 7, is then selected based on the desired likelihood of noise exceeding the threshold, providing a quantitative measure of statistically meaningful correlation.

A manipulation of the coherence maps can be applied to view the coherence with respect to time only. Each of the wavelet coherence maps between uncorrelated velocity and pressure are averaged through its scale component. A display of the scale averaged original $\bar{c}(t)$, mean noise reference $\bar{c}_{mn}(t)$, and threshold $\bar{c}_{th}(t)$ of the coherence between $n_1(t)$ and $pr(t)$ are displayed in Figure 4. The intermittent correlated regions clearly stand out as those surpassing the noise threshold. The applied distribution used to determine g is to the right of the time dependent coherence in Figure 4.

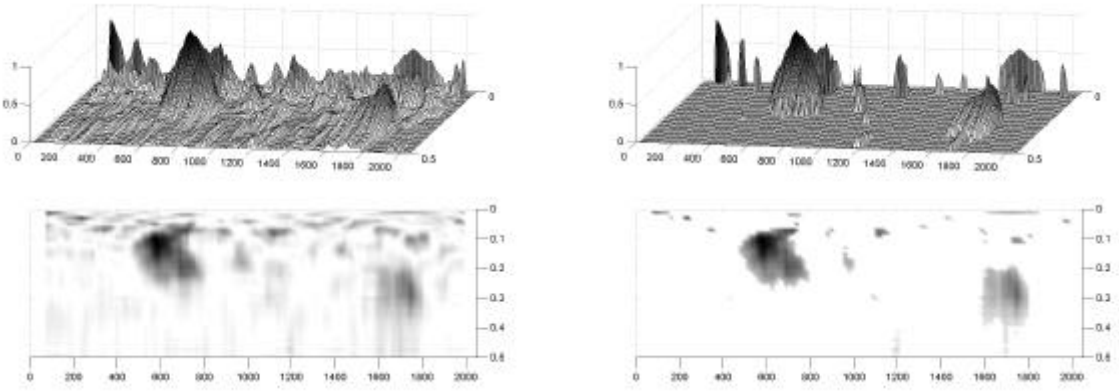

Figure 3. Wavelet coherence map between $n_1(t)$ and $pr(t)$ (left). Wavelet coherence map after filtering with threshold coherence map (right).

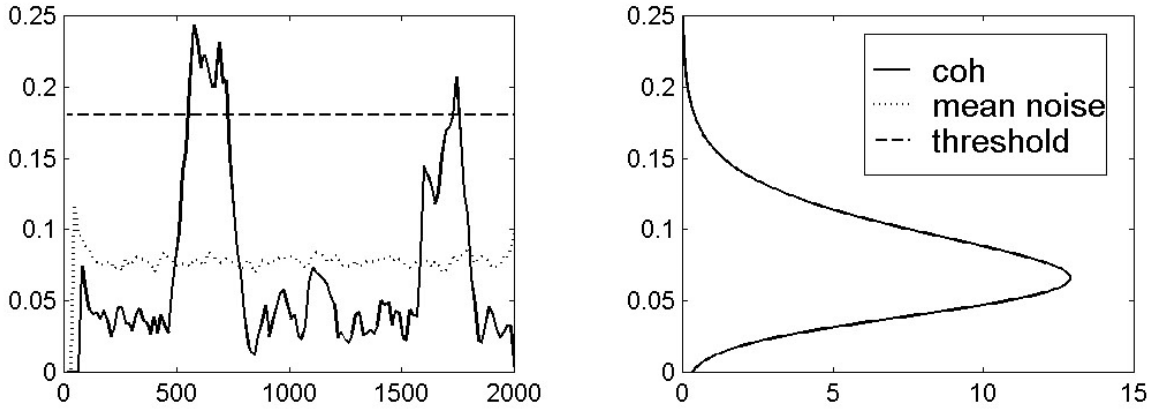

Figure 4. Left: Scale averaged original, mean reference, and threshold coherence maps. Right: distribution of reference noise maps.

3 WAVELET BICOHERENCE MAP

An extension of the wavelet-based spectral estimation of coherence to bicoherence is used identify transient second-order relationships. Wavelet coefficients are used to estimate bicoherence over short time spans, and displayed with respect to both time and frequency. The time-scale wavelet cross-bispectrum, given by

$$B_{xxy}^{W}(a_1,a_2,t)=\int_T W_x(a_1,t)W_x(a_2,t)W_y(a,t)dt\ , \tag{11}$$

where

$$\frac{1}{a}=\frac{1}{a_1}+\frac{1}{a_2},$$

is used in the calculation of the wavelet bicoherence calculation (Powers et al. 1997)

$$\left(b_{xxy}^{W}(a_1,a_2,t)\right)^2=\frac{\left|B_{xxy}^{W}(a_1,a_2,t)\right|^2}{\int_T\left|W_x(a_1,t)W_x(a_2,t)\right|^2dt\int_T\left|W_y(a,t)\right|^2dt}\ . \tag{12}$$

A reference bicoherence map is created to separate statistically relevant correlations from noise. Wavelet bicoherence maps are created between the signal $x(t)$ and multiple independent simulations of the signal $y_s(t)$ statistically identical to $y(t)$ in both PSD and PDF.

The wavelet bicoherence maps between uncorrelated velocity and pressure are averaged to produce a mean noise reference map, $b_{xxy}^{Wmn}(a_1,a_2)$. The standard deviation of the reference maps, $b_{xxy}^{Wst}(a_1,a_2)$, is also calculated. The threshold value of a statistically meaningful correlation is then the addition of the mean and the factored standard deviation of the reference maps

$$b_{xxy}^{Wth}(a_1,a_2)=b_{xxy}^{Wmn}(a_1,a_2)+g\left(b_{xxy}^{Wst}(a_1,a_2)\right). \tag{13}$$

The wavelet bicoherence maps are compared with the threshold bicoherence map calculated in Equation 13 to produce a filtered coherence map according to

$$b_F^W(a_1,a_2,t)=\begin{cases}0 & if \quad b_{xxy}^W(a_1,a_2,t)<b_{xxy}^{Wth}(a_1,a_2,t)\\ b_{xxy}^W(a_1,a_2,t) & if \quad b_{xxy}^W(a_1,a_2,t)>b_{xxy}^{Wth}(a_1,a_2,t)\end{cases}. \tag{14}$$

Validation of the methodology is conducted by creating velocity and pressure signals with known pockets of short duration second-order correlation. Two independent wind velocity signals $(n_1(t),n_2(t))$ are created, each 4096 seconds long and sampled at 1 Hz. The pressure record is created using Equations 9-10 with $G=0.1$. The correlated time segments t in Equation 10 span time ranges from 1000 to 1600 seconds and from 3000 to 3400 seconds.

Equation 12 is applied to determine the bicoherence between $n_1(t)$ and $pr(t)$. The wavelet bicoherence is calculated over 16 time frames evenly spaced over the signals. Four of these maps are shown in Figure 5 (left). The top figures display bicoherence measurements from the two regions that contain second order correlation. The bottom figures display bicoherence measurements from uncorrelated regions. These raw estimates contain noise, making identification of significant correlation difficult to interpret. Figure 5 (right) shows the filtered bicoherence map after application of Equation 14 filters out likely statistical noise. In this example the g value is selected such that probability of noise exceeding the threshold is 10%. 1000 independently simulated pressure records are used to generate the threshold reference map. The correlated time frames are clearly seen in the top two views of the filtered bicoherence map. Most extraneous noise was filtered out in the bottom two segments. A more extensive quantitative study in currently under way.

4 CONCLUSIONS

Wavelet decomposition is used to produce a time-frequency display of the coherence and bicoherence between signals correlated over short periods of time. The noise is filtered from the display map by comparison with a threshold describing likely noise level. This threshold is created by averaging a series of reference correlation maps between one signal and simulations of the second signal. Examples demonstrate that this technique can identify both first and second-order correlation and effectively reduce the presence of noise in the correlation displays.

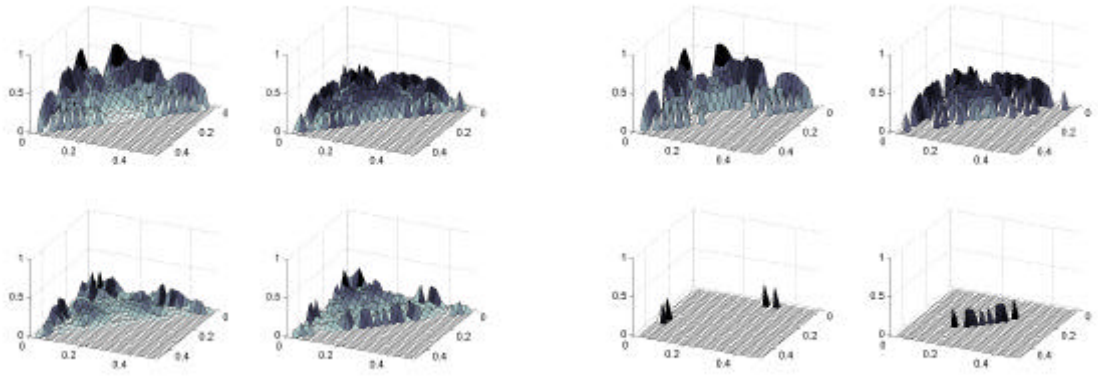

Figure 5. Left: Wavelet bicoherence maps between $n_1(t)$ and $pr(t)$. Top two time segments are correlated time frames, bottom two are uncorrelated time frames. Right: Bicoherence after filtering with threshold bicoherence map.

5 ACKNOWLEDGMENTS

The authors gratefully acknowledge partial support from NSF Grants CMS 99-84635 and CMS 00-85019 for this study.

REFERENCES

Carmona, R., Hwang, W.L. & Torresani, B. 1998. *Practical Time-Frequency Analysis*. Academic Press, San Diego.

Daubechies, I. 1988. Orthonormal basis of compactly supported wavelets. *Comm. pure & appl. maths:* 41: 909-96.

Dunyak, J., Gilliam, X. Peterson, R. & Smith D. 1997. Coherent Gust Detection by Wavelet Transform. *Proceedings of the Eighth U.S. National Conference on Wind Engineering.* The Johns Hopkins University, Baltimore, Maryland.

Farge, M. 1992. Wavelet transforms and their applications to turbulence. *Annual Reviews of fluid mechanics*: 24.

Gurley, K. & Kareem, A. 1999. Application of Wavelet Transforms in Earthquake, Wind, and Ocean Engineering. *Engineering Structures*, 21: 149-167.

Gurley, K. & Kareem, A. 1997a. Analysis, Interpretation, Modeling and Simulation of Unsteady Wind and Pressure Data. *Journal of Wind Engineering and Industrial Aerodynamics*: 69-71: 657-669.

Gurley, K. & Kareem, A. 1997b. Modelling PDFs of non-Gaussian system response. *7th International Conference on Structural Safety and Reliability (ICOSSAR), Kyoto, Japan, November, 1997.*

Gurley, K., Tognarelli, M. and Kareem, A. 1997. Analysis and Simulation Tools for Wind Engineering. *Probabilistic Engineering Mechanics*. 12(1): 9-31.

Kareem, A., Gurley, K., & Kantor, J.C. 1993. Time-Scale Analysis of Nonstationary Processes Utilizing Wavelet Transforms. *Proceedings of the Sixth International Conference on Structural Safety and Reliability (ICOSSAR)*, A.A. Balkema Press, Netherlands, Dec. 1993.

Misiti, M., Misiti, Y., Oppenheim, G., & Poggi, J.M. 1996. *Wavelet Toolbox users guide: for use with MATLAB.* The MathWorks, Inc.

Powers, E.J., Park, S.I., Mehta, S. & Yi, E.J. 1997. Higher-Order Statistics and Extreme Waves. *IEEE Signal Processing Workshop on Higher Order Statistics*: 98-102, July 21-23, Canada.

Strang, G. & Nguyen, T. 1996. *Wavelets and Filter Banks*. Wellesley-Cambridge Press.

Vickery, P.J. 1988. Wind and Wave Loads on Tension Leg Platform: Theory and Experiment. *Ph.D. Dissertation, University of Western Ontario.*